Dielectric Properties of Phase Change Thin Films at Millimeter Waves

Ricardo Carrizales-Juarez, Laure Huitema, Damien Passerieux, Priscillia Daquin, Aurelian Crunteanu

Dielectric Properties of Phase Change Thin Films at Millimeter-Waves

Ricardo Carrizales-Juarez, Laure Huitema, *Member, IEEE*, Damien Passerieux, Priscillia Daquin, and Aurelian Crunteanu, *Member, IEEE*

***Abstract*— We present the characterization of the dielectric permittivity and loss tangent of germanium telluride (GeTe) and germanium antimonium telluride ($Ge_2Sb_2Te_5$- GST) phase change thin-films (less than 1 µm thicknesses) in the millimeter-wave (mmW) domain. The dielectric permittivities in the amorphous (insulator) state of GeTe and GST were measured using two independent differential methods: a wide bandwidth characterization based on the measurement of the propagation constant of a coplanar waveguide and a single frequency characterization based on the measurement of the resonant frequency of a planar resonator. This differential approach allows us to extract the permittivity of the thin film without taking into consideration other parameters of the circuit like the conductivity and the thickness of the metals as well as the losses of the substrate and their permittivity. The extracted mean values range between are 20-22 for the GeTe and 30-34 for the GST. These values are rather constant over the frequency range from 10 GHz to 60 GHz. Additionally, the loss tangent at 30 GHz of both compositions was extracted giving values of $3.4x10^{-2}$ and $3.2x10^{-1}$ for the GeTe and GST, respectively. These values are among the first reported ones regarding the electromagnetic properties of GeTe and GST in this frequency band.**

***Index Terms*— Electromagnetic properties, Germanium antimonium telluride (GST), Germanium telluride (GeTe), Millimeter waves, Phase Change Materials (PCM), Thin films,**

I. Introduction

THE next-generation RF systems (5G and beyond) will face increasing challenges in their performances, such as higher data rates, low latency, higher reliability, higher spectrum efficiency, even lower power consumption and low-cost implementation [1], [2]. As in the case of future 5G front-ends, one way to achieve higher data rates is to span the allocated telecommunication frequencies toward the millimeter waves (frequencies around and greater than 27 GHz) where more bandwidth is available. However, moving up to higher frequencies implies additional problems like higher atmospheric attenuation and diffraction [3]. The next-generation telecommunication systems will therefore need a reconfiguration capability of their front-end constituents (filters, antennas, amplifiers) to optimize their performances at these frequency bands.

Current solutions for realizing reconfigurable antennas or filters are employing semiconductor-based devices (PIN diodes, FET transistors…), functional materials (ferroelectrics, ferrites…) or MEMS devices [4]-[7]. However, the performances of these devices degrade severely or they are not adapted at millimeter wave frequencies. Lately, new reconfiguration paradigms have been proposed, based on the use of agile materials like phase transition materials (PTM) and phase change materials (PCM) [8]-[9]. In particular, germanium telluride (GeTe) phase change materials act as a very efficient RF switch by changing its resistance by more than six orders of magnitude between an amorphous, high-resistivity phase to a low-resistivity, crystalline one, under temperature, electrical or optical excitations. PCM-based RF switches have high isolation in the OFF state of up to 20 dB and low insertion loss in the ON state of less than 3 dB (depending on the size of the PCM switch), good power handling up to 34 dBm [10], low power consumption and a figure of merit greater than or equal to current switching technologies based on semiconductor devices [11]-[14]. Other compositions such as germanium antimonium telluride ($Ge_2Sb_2Te_5$, abbreviated GST) or antimonium telluride (SbTe) have also been studied as they have similar properties to those of GeTe compositions [15-16]. As in the case of their early applications as non-volatile memory devices, the operation of these materials in the RF domain is based on the ability of PCM materials to be switched using short electrical [12], [13] or optical [11], [13] pulses between an OFF state (amorphous/ insulating state) and an ON state (crystalline/ conducting material) [11]-[13].

The bi-stability of RF-PCM devices is a key advantage of this technology. Indeed, the switch does not require a permanent bias to be maintained in a specifically prepared state (ON or OFF). We have previously demonstrated bi-stable switching functions based on phase change materials using electrical or optical actuation [11], [12] and confirmed the potential of these materials to realize more complex agile

This work was supported by the French National Center for Spatial Studies (CNES) and University of Limoges. (*Corresponding author: Ricardo Carrizales-Juarez.*)

Ricardo Carrizales-Juarez is with the National Center for Spatial Studies (CNES) and, the XLIM Research Institute, CNRS/ University of Limoges, 87060, 123 avenue Albert Thomas, Limoges, France (email: ricardo.carrizales@xlim.fr)

Laure Huitema is with the XLIM Research Institute, CNRS/ University of Limoges, 87000,123 avenue Albert Thomas, Limoges, France (e-mail: laure.huitema@unilim.fr).

Damien Passerieux is with the XLIM Research Institute, CNRS/ University of Limoges, 87060, 123 avenue Albert Thomas, Limoges, France (email: damien.passerieux@xlim.fr)

Priscillia Daquin is with the National Center for Spatial Studies (CNES), 31000, 18 avenue Edouard Belin, Toulouse, France (email: priscillia.daquin@cnes.fr)

Aurelian Crunteanu is the XLIM Research Institute, CNRS/ University of Limoges, 87060, 123 avenue Albert Thomas, Limoges, France (email: aurelian.crunteanu@xlim.fr)

functions, such as filters [17] or frequency reconfigurable antennas [18].

For the design of complex RF functions (filters, antennas) integrating this type of materials, it is necessary to know their microwave dielectric properties, in each of their states. Some compositions of PCM have already been characterized for frequencies less than 3 GHz and in the THz domain [19]-[21]. Unfortunately, there is no available data on the electromagnetic properties of PCMs at millimeter wave frequencies. Additionally, since the thickness of the PCM compositions obtained on substrates is in the order of hundreds of nanometers, a characterization by means of conventional techniques can be difficult at higher frequencies, as shown in [19], [21] where the fluctuations in the permittivity values can go as high as 20% for some compositions.

We present here the broadband electromagnetic characterization of very thin layers of GeTe and $Ge_2Sb_2Te_5$ phase change materials (less than 1 µm) using two independent methods, allowing to extract the effective dielectric permittivity of specifically designed test devices integrating GeTe and GST in amorphous state. The dielectric permittivity of these compositions in amorphous state were extracted by comparing the measurements of their millimeter-wave performances with device retro-simulations using either analytical methods or full-wave electromagnetic simulations using CST-Microwave Studio. However, to accurately extract the permittivity values, one must also precisely know other parameters of the devices used for the characterization like the losses of the substrate and permittivity or the thickness and conductivity of the metallic layers, for this reason, we also propose a differential approach measure to eliminate the necessity of knowing these parameters.

II. Methodology and Theory of Permittivity Extraction

Current techniques for measuring the dielectric permittivity are mostly based on cavity resonant techniques allowing accurate extraction of the permittivity value and the loss tangent of the material [22], [23]. However, these methods can only extract the permittivity of the material at a single frequency and the results are prone to substantial errors when the thickness of the layer to be measured is in the order of hundreds of nanometers, unless the permittivity of the material is very high. Alternative methods such as [24], [25] involve the measuring of transmission and reflection coefficients in a waveguide charged by the material to be characterized. However, these methods require a substantial quantity of material (enough to fill the waveguide and sufficiently thick) and proper installation of the propagating mode in the structure.

Other methods such as the one presented in [26] allows to extract the permittivity of thin films over a wide bandwidth by measuring the S-parameters of a single CPW integrating a thin layer of ferroelectric material. Then, the permittivity of the ferroelectric material can be extracted by comparing the propagation constant of the CPW to the one calculated by the method of Spectral Domain Approach. However, the technique requires a full knowledge of the electromagnetic properties of the structure in which the thin film is integrated, such as the conductivity of the metal or the permittivity and losses of the substrate at the measurement frequencies.

Our proposed approach is the extraction of the effective permittivity of specific planar devices fabricated on bare substrates and, additionally, on substrates covered with the thin PCM film to be characterized. Assuming that equivalent fabricated devices on the two types of substrates are identical and knowing the thickness of each layer in the stacks, then the effective permittivity variation corresponding to the dissimilar substrates should only reflect the influence of the PCM layer. This assumption can be satisfied if the devices (with and without a thin PCM film) are fabricated on the same substrate with the same metallic layer. Using this differential measurement procedure for a similar device fabricated on a bare substrate and on a substrate covered with a PCM layer, we can then evaluate the permittivity of the PCM material without actually considering the losses of the metallic structure of the devices. We, therefore, proposed two complementary methods, one for a single frequency evaluation and other for a wide frequency evaluation based on:

1) a comparison between the modification of the resonant frequency of a simple stub resonator operating in the mmW domain with and without a PCM pattern integrated in the stub's structure (Fig. 1(a)), and
2) a differential measurement of the propagation constant of a simple coplanar waveguide transmission line (CPW) fabricated on a bare substrate and on the same substrate covered by a thin PCM layer (Fig. 1(b)) measured using the mathematical development of the "Through-Reflect-Line" method.

The cross section of a bare CPW is shown in Fig. 1(c) while the cross section of a CPW integrating a PCM layer is shown in Fig. 1(d).

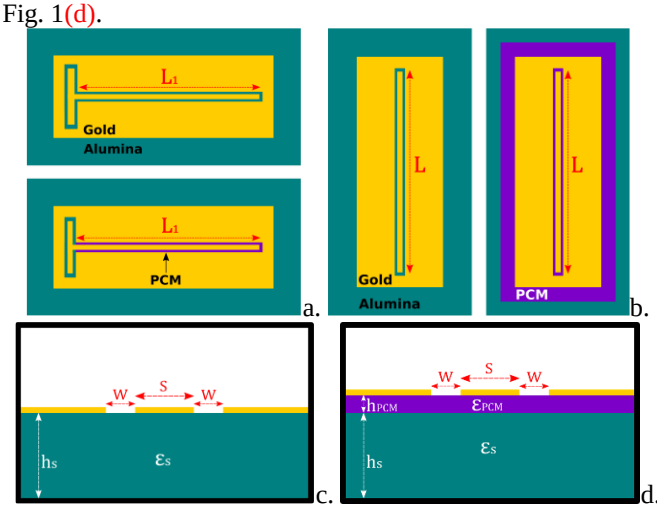

Fig. 1. (a) Design of mmW stub resonators without a PCM (up) and integrating a PCM pattern (down). (b) Example of a CPW line fabricated on an alumina substrate (left) and on a PCM/ alumina layer (right). (c) Cross-section cut of a CPW on an alumina substrate. (d). Cross-section cut of a CPW on a PCM/Alumina substrate.

A. Resonator Frequency Method

In the first case, the stub will resonate at a particular frequency given by

$$f_r = \frac{c_0}{\tau.\sqrt{\varepsilon_{eff}}.L_1}, \quad (1)$$

where τ is equal to 2 for a series type resonance and equal to 4 for a parallel type resonance, L_1 is the length of the stub, c_0 is the speed of light and ε_{eff} is the effective permittivity of the line which is a function of the substrate permittivity and its thickness.

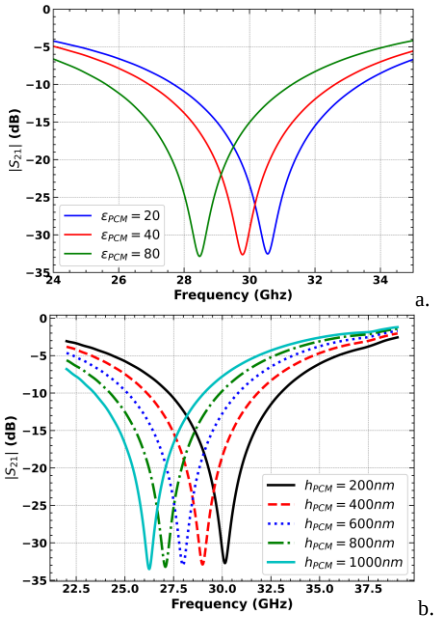

Fig. 2. (a) Variation of the stub's resonant frequency as a function of the permittivity of the GeTe layer. (b) Variation of the resonant frequency of the stub as a function of the GeTe layer thickness.

By adding a layer of PCM, the effective permittivity of the resonator will be modified and the resonance frequency of the resonator will shift as a function of the permittivity of the PCM, as shown in the Fig. 2(a). The change in the ε_{eff} is also dependent on the PCM layer thickness, meaning that the resonant frequency values will depend on these two parameters, as shown in Fig. 2(b). The permittivity of the PCM layer at the stub's resonant frequency can be then straightforwardly extracted by analytical and electromagnetic retro-simulations of the devices and knowing the dimensions of the stub, the thickness of the PCM layer and by measuring the resonance frequency of the device.

B. Transmission Line Method

The second method employed for extracting the PCM permittivity over a wide frequency band is based on the evaluation of the complex propagation constant γ of a CPW line fabricated on a bare substrate and on a substrate covered by a PCM layer, using the multiline Thru-Reflect-Line (TRL) technique [27]. The analytical model of the TRL technique allows to calculate the propagation constant of the transmission line by measuring the Line and Thru standards (Fig. 3). The cascade parameters of an ideal transmission line are given by:

$$[L^i] = \begin{bmatrix} e^{-\gamma.l_i} & 0 \\ 0 & e^{+\gamma.l_i} \end{bmatrix} \quad (2)$$

where l_i is the length of the line and γ is the complex propagation constant of the line which can be calculated using the eigenvalues of (2). In practice however, the measurement of a transmission line produces the cascade matrix:

$$[M^i] = [X].[T^i].[Y] \quad (3)$$

where X and Y are the cascade parameters of the (unknown) "error boxes" at the detector plane and T^i is the actual matrix of the transmission (non-ideal) line given by:

$$T^i = (I + \delta^{1i})L^i(I + \delta^{2i}) \quad (4)$$

where [I] is the identity matrix and $[L^i]$ is the ideal cascade matrix of the transmission line. The terms $[\delta^{1i}]$ and $[\delta^{2i}]$ represent small perturbations at port 1 and port 2, respectively, on the ideal transmission line described in [27]. Therefore, the extraction of the propagation constant from a single line measurement is not so straightforward.

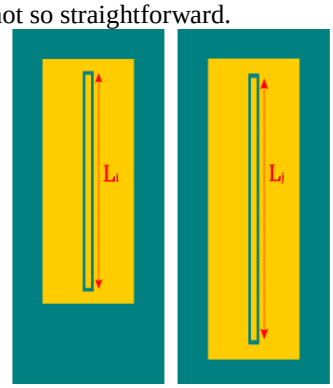

Fig. 3. Transmission lines geometry for the standards "Thru" (left) and "Line" (right) for the TRL method.

Measuring two lines (or two standards) $[L^i]$ and $[L^j]$ of lengths l_i and l_j will produce the matrices $[M^i]$ and $[M^j]$ which can be combined to form the following matrix equation:

$$[M^{ij}].[X] = [X].[T^{ij}] \quad (5)$$

where:

$$[M^{ij}] = [M^j].([M^i])^{-1} \quad (6)$$

and:

$$[T^{ij}] = [T^j].([T^i])^{-1} \quad (7)$$

If the perturbations on the line are small, the T matrix can be expressed as:

$$[T^{ij}] \approx [L^{ij}] + [\epsilon^{ij}] \quad (8)$$

where:

$$[L^{ij}] = \begin{bmatrix} e^{-\gamma.(l_j - l_i)} & 0 \\ 0 & e^{+\gamma.(l_j - l_i)} \end{bmatrix} \quad (9)$$

and $[\epsilon^{ij}]$ is a small error term which can be neglected if the perturbations on the line are small enough. Once again, the propagation constant of the line can be calculated from (9) using the eigenvalues of the matrix and the length difference of the two measured transmission lines.

However, as mentioned previously, on practice we measured the matrices $[M^i]$ and $[M^j]$. On the other hand, in [27] it is demonstrated that the eigenvalues of the $[M^{ij}]$ and $[T^{ij}]$ matrices are the same (although their eigenvectors are different), therefore calculating the eigenvalues of $[M^{ij}]$ provides a good approximation of the propagation constant of the line provided that the error terms in (8) are small enough. The eigenvalues of $[M^{ij}]$ are calculated using:

$$\lambda^{ij}_{1,2} = \frac{1}{2}\left[(M^{ij}_{11} + M^{ij}_{22}) \pm \sqrt{(M^{ij}_{11} - M^{ij}_{22})^2 + 4.M^{ij}_{12}.M^{ij}_{21}}\right] \quad (10)$$

where M_{mn} are the element of the matrix $[M^{ij}]$. We can associate one eigenvalue to the negative exponential in (2) and the other with positive exponential. This estimation can be improved by taking a simple average of the eigenvalues given by:

$$\lambda^{ij} = \frac{1}{2}\left[\lambda^{ij}_1 + 1/\lambda^{ij}_2\right]. \quad (11)$$

Then, the propagation constant can be calculated using the following equation:

$$\gamma^{ij} = \frac{\ln(\lambda^{ij})}{(l_i - l_j)} \approx \gamma + \Delta\gamma^{ij} \quad (12)$$

where γ is the propagation constant of the line and $\Delta\gamma^{ij}$ is a linear error term described in [27] which can be neglected if the error terms are small or by maximizing the difference between the transmission lines, according to [27].

Once γ is known, one can extract the effective permittivity of the transmission line by using:

$$\varepsilon_{eff} = \left(\frac{\beta}{k_0}\right)^2, \quad (13)$$

where k_0 is the wave number and β is the imaginary part of the complex propagation constant. Additionally, from the real part of the propagation constant, the total losses of the CPW can be extracted. For a CPW, the total losses α_t of the line are expressed as:

$$\propto_t = \propto_c + \propto_s + \propto_{PCM} \quad (14)$$

where α_c, α_s and α_{PCM} are the losses due to conductors, the substrate and PCM, respectively.

As in the previous case, the effective permittivity is a function of the substrate and PCM layer permittivity and thickness. The measurement of the physical dimensions of the line and of the PCM layer thickness will allow us to obtain their permittivity ε_{PCM}.

In this work, we employed an additional analytic method based on the equivalent network representation [28], [29] which allows calculating the effective permittivity of the CPW. Moreover, by electromagnetic retro simulations of the measured scattering parameters of the CPW line the previous analytical values will be validated.

The fundamental theory on the "Equivalent Network Representation" can be found in [28], [29] and allows to derive the integral equations for electromagnetic boundary problems by applying the Kirchhoff and Ohm's law to a circuit representation of the boundary value problem in question (called "Equivalent network") where voltages represent the tangential components of the electric field at the boundaries and currents represent the density currents at the boundaries. This integral equation is then solved by the application of the Galerkin method [29], [30] which produces an equation that can be solved for the propagation constant β.

The advantage of this analytical method is that the model is considering the anisotropy of the substrate, multiple layers, the thickness of the metal and the losses of the conductors [30], [31]. Nonetheless, in this work we will be using a simpler formulation where the conductor is a lossless thin layer as we are only interested in the shift in the effective permittivity caused by the addition of a thin layer of PCM.

Thus, following the development in the Appendix I, by developing (32), we arrive to

$$\sum_n |\langle \overrightarrow{g_e} | f_n^{TE} \rangle|^2 \left(\left(Y_{1,n}^{TE} + Y_{2,n}^{TE}\right) + \left(n\pi/\beta a\right)^2 \left(Y_{1,n}^{TM} + Y_{2,n}^{TM}\right) \right) = 0 \quad (15)$$

where

$$|\langle \overrightarrow{g_e} | f_n^{TE} \rangle|^2 = \frac{8}{a} \frac{\beta^2 w^2}{\left(\frac{n\pi}{a}\right)^2 + \beta^2} \left(\sin\left(n\frac{\pi(s+w)}{2a}\right)\right)^2 \left(sinc\left(n\frac{\pi w}{2a}\right)\right)^2 \quad (16)$$

the expression for the free space admittances for the TE and TM modes $Y_{1,n}^{TE}$ and $Y_{1,n}^{TM}$ are given by:

$$Y_{1,n}^{TE} = \frac{p_{1,n}}{j2\pi f \mu_0} \coth\left(p_{1,n}(b-h)\right) \quad (17)$$

and

$$Y_{1,n}^{TM} = \frac{j2\pi f \varepsilon_0}{p_{1,n}} \coth\left(p_{1,n}(b-h)\right) \quad (18)$$

where $h = h_s$ for a single layer substrate and $h = h_p + h_s$ for a multilayer substrate. The expression for $p_{1,n}$ is given by

$$p_{1,n} = \sqrt{\left(\frac{n\pi}{a}\right)^2 + \beta^2 - {k_0}^2}. \quad (19)$$

The expression for the admittance in the substrate region $Y_{2,n}^{TE}$ and $Y_{2,n}^{TM}$ is more complicated for a multilayer substrate as we need to consider a third region (The region where the PCM exist). We will note $Y_{2s,n}^{TE}$ and $Y_{2s,n}^{TM}$ the admittances for a single layer case and $Y_{2m,n}^{TE}$ and $Y_{2m,n}^{TM}$ the admittances for a multilayer case. For a single layer substrate, the admittances of the substrate region are given by

$$Y_{2s,n}^{TE} = \frac{p_{2,n}}{j2\pi f \mu_0} \coth\left(p_{2,n}h_2\right) \quad (20)$$

and

$$Y_{2s,n}^{TM} = \frac{j2\pi f \varepsilon_0 \varepsilon_r}{p_{2,n}} \coth\left(p_{2,n}h_2\right) \quad (21)$$

where

$$p_{2,n} = \sqrt{\left(\frac{n\pi}{a}\right)^2 + \beta^2 - \varepsilon_r {k_0}^2}. \quad (22)$$

For a multilayer substrate, the substrate and PCM admittances for the TE and TM modes are given by

$$Y_{2m,n}^{TE} = \frac{p_{3,n}}{j2\pi f \mu_0} \left[\frac{\frac{p_{3,n}}{j2\pi f \mu_0} + Y_{2s,n}^{TE} \coth(p_{3,n}h_1)}{Y_{2s,n}^{TE} + \frac{p_{3,n}}{j2\pi f \mu_0} \coth(p_{3,n}h_1)} \right] \quad (23)$$

and

$$Y_{2m,n}^{TM} = \frac{j2\pi f \varepsilon_0 \varepsilon_{PCM}}{p_{3,n}} \left[\frac{\frac{j2\pi f \varepsilon_0 \varepsilon_{PCM}}{p_{3,n}} + Y_{2s,n}^{TM} \coth(p_{3,n}h_1)}{Y_{2s,n}^{TM} + \frac{j2\pi f \varepsilon_0 \varepsilon_{PCM}}{p_{3,n}} \coth(p_{3,n}h_1)} \right] \quad (24)$$

where

$$p_{3,n} = \sqrt{\left(\frac{n\pi}{a}\right)^2 + \beta^2 - \varepsilon_{PCM} {k_0}^2}. \quad (25)$$

With this set-up, (15) can be solved for β using numerical techniques. Once β is known, one can calculate the effective permittivity of the line using (13) for any frequency, for a single and multilayer case.

C. *Extraction Of The Permittivity Of The Pcm Layer From The Effective Permittivity Of The CPW Line.*

As stated in the previous section, a direct and accurate extraction of the permittivity of the PCM using a transmission line geometry presented in Fig. 1(d) will require a full knowledge of some properties such as conductivity of the metal layer, its thickness, the permittivity of the substrate and its dielectric losses. The roughness of the PCM material must be also known, as it may modify the effective permittivity of the line and the conductivity of the metallisation [33], [34].

Therefore, to accurately extract the permittivity of the PCM layer we propose a differential measure using the following procedure:

1. We set the equation

$$\varepsilon_{eff}(f, \varepsilon_{Substrate}) - \varepsilon_{eff,m}(f) = 0 \quad (26)$$

where ε_{eff} is the effective permittivity calculated from (15) and (13) or by electromagnetic simulation of a CPW fabricated on a bare substrate while $\varepsilon_{eff,m}$ is the measured effective permittivity extracted from the CPW lines using the TRL procedure or from the

resonance frequency of a stub resonator fabricated on a bare substrate. Both values are calculated for a single frequency *f*.

2. Equation (26) is then solved for $\varepsilon_{Substrate}$.
3. We set another equation

$$\varepsilon_{eff-PCM}(f, \varepsilon_{Substrate}, \varepsilon_{PCM}) - \varepsilon_{eff-PCM,m}(f) = 0 \quad (27)$$

where $\varepsilon_{eff\text{-}PCM}$ is the effective permittivity calculated from (15) and (13) or by electromagnetic simulation for a CPW fabricated on the same substrate covered by a PCM layer and $\varepsilon_{eff\text{-}PCM,m}$ is the measured effective permittivity extracted from the CPW lines using the TRL procedure or from the resonance frequency of a stub resonator fabricated on a similar bilayer substrate. Both values are calculated for a single frequency *f*.

4. Equation (27) is then solved for ε_{PCM} using the $\varepsilon_{Substrate}$ calculated in step 2.

This approach allows us to calculate the permittivity of the PCM just from the change in the effective permittivity of the CPW lines and resonators from adding a layer of PCM without needing to consider other parameters described previously (like the thickness of the metal, the roughness of the substrate and the losses of the substrate and metal).

Note that $\varepsilon_{Substrate}$ calculated from (26) using the analytical method is not necessarily the permittivity of the substrate, as this formulation does not take into consideration the losses and the thickness of the metal or any other perturbation in the CPW line. Nonetheless, if the losses in the lines are negligible, then the extracted $\varepsilon_{Substrate}$ can be a good approximation of the real permittivity of the substrate. As an example, at 30 GHz, the extracted ε_s of the alumina substrate from the 3D electromagnetic simulation is 9.47, while the extracted ε_s from the analytical method is 9.39. Although the extraction from the electromagnetic simulation approach takes a considerable amount of time due to the need of a finer mesh in the boundary of the metallisation.

D. Extraction Of The Loss Tangent Of The Pcm Layer From The Total Losses Of The CPW Line.

In a similar way to the extraction of the permittivity, accurate extraction of the losses of the PCM will also require a full knowledge of the electromagnetic properties of the structures in particular the losses of the metal and substrates. However, since the CPW with and without PCM are fabricated over the same substrate and during the same process of metal deposition, the terms α_c and α_s should be, in average, similar for both type of devices. Therefore, any supplementary losses in the CPW must be necessarily introduced by the PCM layer.

To accurately extract the loss tangent of PCM we also propose a differential method to extract the losses of the PCM by solving the equation:

$$\propto_{PCM}(f, tan(\delta)) - (\propto_{t-PCM}(f) - \alpha_t(f)) = 0 \quad (28)$$

where $\alpha_{t\text{-}PCM}$ and α_t are the total losses measured by the TRL method with and without a PCM layer respectively. Since we do not dispose of an analytical model for evaluating the losses of a bi-layer CPW, (28) is solved using 3D electromagnetic simulations.

III. Device Fabrication and Measurements

We fabricated four samples integrating the devices presented on Fig. 1. Three devices were fabricated by deposition of thin layers of GeTe using the DC magnetron sputtering of a 50:50 GeTe target, on 25×25 mm^2 substrates. Since the method of dielectric properties extraction developed in section II requires us to first calculate the permittivity of the substrate on which the PCM is obtained from the effective permittivity of the line, the use of an anisotropic material (e.g. sapphire) will complicate a precise extraction of the PCM permittivity. Therefore, to accurately extract the permittivity of the PCM layer, we favor the use of isotropic materials. Thus samples 1 and 2 were fabricated on alumina substrates while sample 3 was fabricated on a SiO_2 substrate. The magnetron sputtering technique can be used to obtain PCM layers up to several micrometers in thickness, however the time required to film's fabrication with these thicknesses can be considerable long. We therefore explored films properties with thicknesses under or around micrometer range, which were previously show to be adapted for integration in devices for millimeter-wave domain [10]-[15]. ~~This magnetron sputtering technique can be used to depose PCM layers up to several micrometers in thickness, however the time required to depose layers in the micrometer range can be considerable long, therefore we decided to explore the sub micrometer range.~~ Samples 1 and 3 correspond to devices with a GeTe layer having a thickness of 500 nm and sample 2 correspond to devices with GeTe layer of 800 nm.

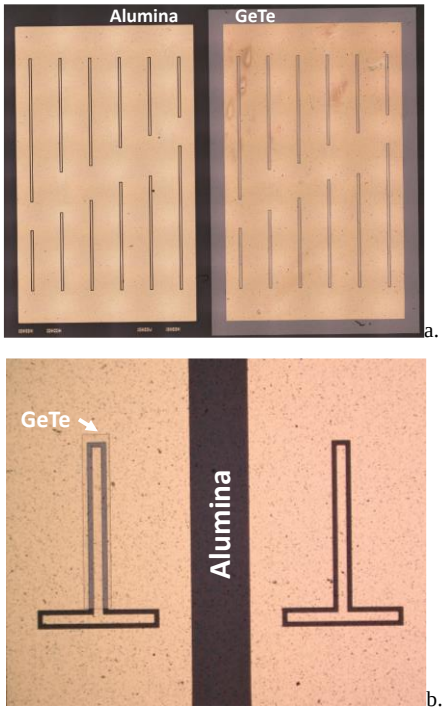

Fig. 4. (a) CPW lines fabricated over a layer of alumina (to the left) and over a layer of GeTe/alumina (to the right). (b) Stub resonators fabricated over a layer of alumina (to the right) and a layer of GeTe/alumina (to the left)

The fabricated circuits corresponding to the two types of designs shown in Fig. 1(a) and Fig. 1(b) are shown on Fig. 4(a) and Fig. 4(b), respectively. For each sample with different PCM and thicknesses, two sets of seven stub resonators (with and without a layer of PCM) were fabricated. The stubs' lengths L

have dimensions of 0.8 mm, 0.9 mm, 1.0 mm, 1.1 mm, 1.2 mm, 1.3 mm and 1.4 mm, corresponding to specific resonant frequencies in the band 20 to 40 GHz on the alumina substrate and 30 to 50 GHz on the SiO_2 substrate. The ground planes aside the stub resonators were connected using gold wire bonding (not shown on Fig. 4(b)) for suppressing the propagation of higher order modes and prevent the structure to radiate [35], [36].

Two sets of CPW lines (on the bare substrate and on a PCM sub-layer) were also realized on each of the samples mentioned before. Three sets of similar lines with different lengths where designed and fabricated to introduce phase variations around 90° between specific pairs of lines at 30 GHz (≈ 1.2 mm, on the alumina substrate). The lengths L of the transmission lines are L_1 = 2.0 mm, L_2 = 2.4 mm, L_3 = 3.2 mm, L_4 = 3.6 mm, L_5 = 3.8 mm and L_6 =4.6 mm. The pairs used for evaluation of the propagation constant are the lines L_1-L_3, L_2-L_4 and L_5-L_6.

The RF characteristics of the investigated devices (stubs and CPW lines) were measured in the 100 MHz- 67 GHz range using Ground-Signal-Ground (GSG) Cascade probes connected to a vector network analyzer (ZVA Rohde & Schwarz) allowing to extract the experimental S-parameter matrices, as shown in Fig. 5.

The DC conductivity of the PCM layer was measured on a PCM layer deposed over a sapphire substrate using the 4-Points probe method. The conductivity in the amorphous state was evaluated at 0.02 S/m while the conductivity at crystalline state (transformed from amorphous state using a heating plate) was evaluated at 2.3×10^5 S/m.

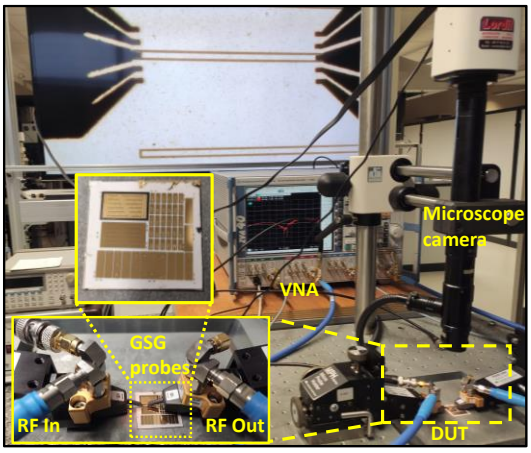

Fig. 5. Image of the test system used to measure the RF performance of all samples (VNA- vector network analyzer, DUT-device under test).

IV. Extraction of PCM layers permittivity

A. Resonators Analysis

The effects of adding a thin layer of GeTe within a stub resonator structure is clearly shifting its resonant frequency, as shown on the experimentally recorded responses of a typical stub resonator device in Fig. 6. By measuring the resonant frequency of both resonators (with and without the GeTe layer) and using (1) to calculate the effective permittivity for each device, we can deduce the permittivity of the PCM layer generating the change in the effective permittivity. The PCM permittivities were extracted using the proposed analytical method and the 3D electromagnetic simulation of the devices (the latter also takes into consideration the conductivity of the metal and its thickness). Since the PCM layer is very thin with respect to size of the substrate and smaller than the thickness metallisation, the 3D electromagnetic simulation requires a very fine mesh at the boundaries of the PCM. To solve the propagation constant, we profit of the "waveguide port" utility of CST Microwave using the hexahedral mesh and a time domain simulation.

The results presented in Table I for devices with stubs having different dimensions show that the permittivity values obtained using both methods agree very well. Most of the values in Table I are close to 21, however the extracted permittivity from the resonators of length 1.2 and 0.9 mm are far from 21, this dispersion between permittivity values reported in Table I can be explained by variations on the thickness of the PCM layer or by undesirable perturbations due the welding of gold wires used to equalize the ground planes as well as inaccuracies in the reading of the resonance frequency. In fact, as shown in Fig. 2(b) and demonstrated in Appendix II, the resonance frequency is sensible to thickness of the PCM layer, therefore any inhomogeneity in the thickness of the layer will cause a change in the resonance frequency of the resonator, this situation is aggravated by the rough surface of the alumina substrate in which the PCM layer is deposed.

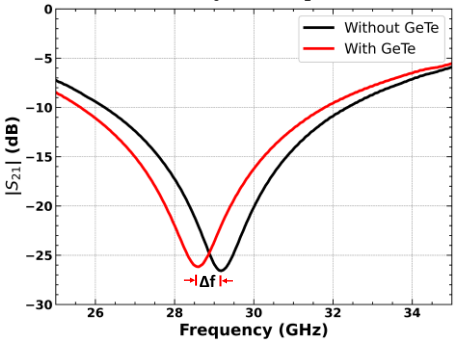

Fig. 6. Measured S_{21} parameters of a stub resonator with length of 1.3 mm showing clear changes in the parallel resonant frequency due to the addition of a thin layer of GeTe.

TABLE I.

COMPARISON OF THE EXTRACTED PERMITTIVITY OF THE GETE USING THE ANALYTICAL METHOD AND 3D ELECTROMAGNETIC SIMULATION USING CST FOR ALL RESONATORS CORRESPONDING TO SAMPLE 1 (ALUMINA SUBSTRATE, 500-NM THICK GETE LAYER)

Resonator length (mm)	Resonant frequency (GHz)		GeTe Permittivity	
	Without GeTe	With GeTe	3D EM Simulation	Analytical method
1.4	23.11	22.67	22.0	21.9
1.3	24.89	24.45	20.6	20.9
1.2	26.83	26.42	17.7	17.6
1.1	29.28	28.77	20.8	21.0
1.0	32.16	31.61	20.7	19.8
0.9	35.68	35.23	18.1	18.4

TABLE II

MEAN VALUES OF THE GETE AND GST PERMITTIVITIES EXTRACTED FROM THE ENTIRE SETS OF STUB RESONATORS, FOR ALL SAMPLES 1-4

Resonator length (mm)	GeTe			GST
	Sample 1	Sample 2	Sample 3	Sample 4
1.4	22.6	19.6	18.5	33.2

1.3	21.6	19.9	19.2	34.8
1.2	17.6	22.2	23.9	36.0
1.1	21.7	22.4	20.2	28.2
1.0	21.33	18.2	15.5	30.8
0.9	18.4	19.3	17.3	28.3
0.8	----	23.9	24.3	38.6

The results on GeTe permittivity in Table II shows the permittivity of the GeTe and GST compositions for the entire set of resonators. For the GeTe compositions we can observe that most of the extracted values are around 21, however there are certain values that are far away from the mean value which (as stated previously) can be attributed to variations on the thickness of the PCM layer and the bonding wires. Nonetheless, these values agree very well with the ones found in [19] where the permittivity of the GeTe was evaluated to be around 24.4 using the impedance spectroscopy method from 10 MHz up to 100 MHz. Other measurements in the THz domain [21] suggest that the permittivity of the GeTe is around 19 at 250 GHz. These results suggest that permittivity of the GeTe has little dispersion in the frequency band from 10 MHz up to 250 GHz. The same conclusions can be made for the GST composition permittivity, where the value reported by [19] is around 34 for frequencies from 10 MHz up to 100 MHz.

B. Transmission Line Analysis

The measured S_{21} parameters of the six CPW fabricated over a bi-layer of alumina or SiO_2 substrate and the GeTe film are shown in Fig. 7(a) and Fig. 7(b), respectively. The curves measured on an alumina substrate are noisier than the ones measured on a SiO_2 substrate, due to the higher roughness of the alumina substrate. Therefore, before applying the methodology described in section II, the data were filtered by applying a Savitzky-Golay filter [37] using a third-degree polynomial with a window of 2000 frequency points. This filter was applied separately to the real and imaginary parts of the measured S parameters of each line. The results of the post-processed measured S parameters for the L6 line are displayed in Fig. 8(a) and Fig. 8(b) for an alumina and SiO_2 substrate, respectively. From both figures, it can be seen that the noise has been filtered out while preserving the overall trending of the S_{21} curve (as clearly shown in Fig. 8(b)).

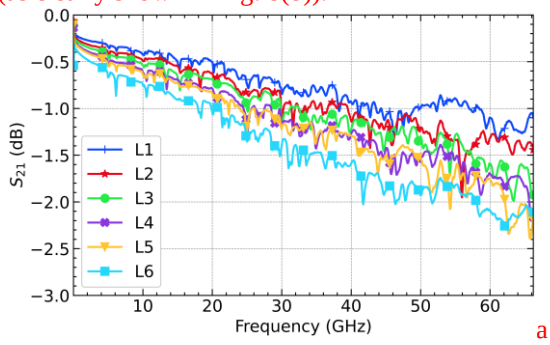

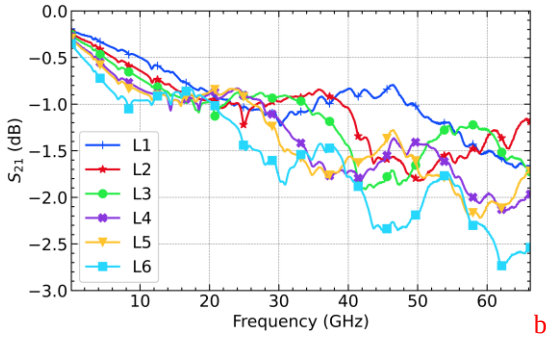

Fig. 7. (a) Measured S_{21} parameters of all the CPW lines fabricated on an alumina substrate integrating a thin layer of GeTe (sample 2) and (b) similar parameters of the CPW lines fabricated on a SiO_2 substrate integrating a thin layer of GeTe (sample 3).

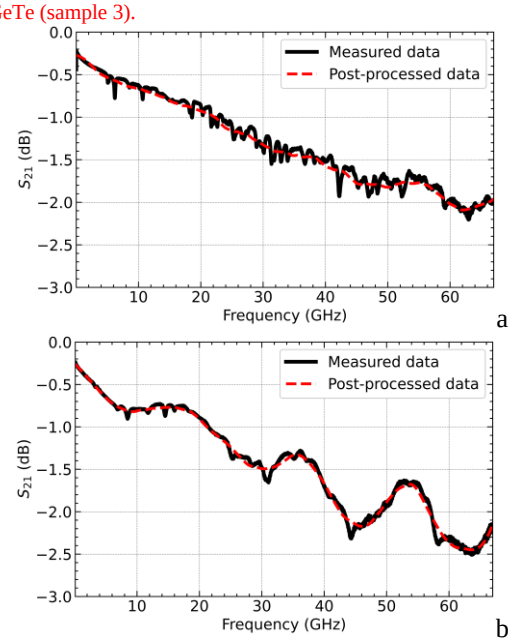

Fig. 8. (a) Measured S_{21} parameters of L6 line in sample 2 (alumina substrate) with a thin layer of GeTe before and after post-processing and (b) similar result for the L6 CPW line with a thin layer of GeTe on sample 3 (SiO_2 substrate).

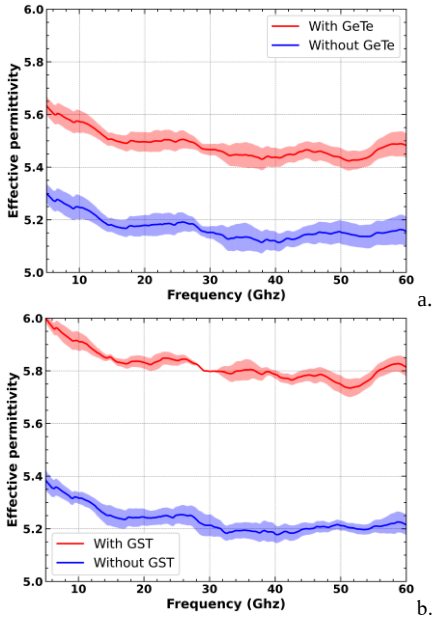

Fig. 9. (a) Comparison of the mean effective permittivity values extracted using the TRL method from the fabricated transmission lines on an alumina substrate,

with and without a GeTe layer of 800 nm (sample 2). (b) Comparison of the mean effective permittivity values extracted using the TRL method from a CPW with and without a GST layer of 800 nm on an alumina substrate (sample 4).

The effect of adding a thin layer of GeTe and GST under the transmission line devices and their influence on the effective permittivity of the fabricated coplanar waveguide is shown on Fig. 9(a) for GeTe and on Fig 9(b), for GST respectively. The mean value of CPWs effective permittivity is represented as a function of frequency in the 5-60 GHz frequency domain and was evaluated using the analytical method from each of the two sets of three pairs of CPW lines (lengths L_1-L_3, L_2-L_4 and L_5-L_6). The standard error of the mean values (see Appendix II) calculated at every frequency value is also shown for each permittivity trace. One can notice that the addition of PCM layers (GeTe or GST) are only proportionally increasing the values of ε_{eff} without changing its overall shape, suggesting that the permittivities of both GeTe and GST are rather constants over the investigated frequency band.

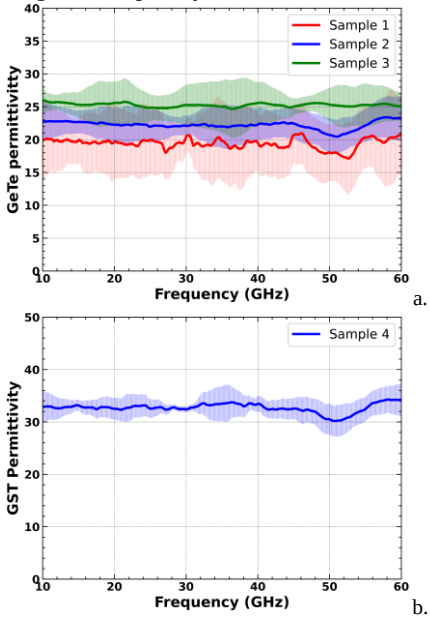

Fig. 10. (a) Mean and dispersion values of the extracted permittivity of GeTe using the analytical method for all samples integrating GeTe (1-3). (b) Mean and dispersion values of the extracted GST permittivity using the analytical method.

Table III shows a comparison of the extracted permittivity of the GeTe layer using both the analytical method and 3D electromagnetic simulations for sample 2 (800 nm thick GeTe layer). It can be seen that both methods agree very well, especially at low frequencies.

Following the same approach and using the analytical estimation method, Table IV summarizes the values of the extracted permittivity for both PCM compositions and for all fabricated samples.

TABLE III
COMPARISON OF THE EXTRACTED PERMITTIVITY OF THE GETE FOR THE CPW LINES OF SAMPLE 2 (800 NM THICK GETE ON ALUMINA SUBSTRATE) USING THE ANALYTICAL METHOD AND THE 3D ELECTROMAGNETIC SIMULATION

Frequency	Effective permittivity		GeTe permittivity	
	With GeTe	Without GeTe	3D EM Simulation	Analytical method
20	5.17	5.50	23.2	22.2
30	5.15	5.47	22.3	21.7
40	5.10	5.42	21.7	21.6
50	5.13	5.43	20.4	20.1
60	5.14	5.47	21.0	22.7

TABLE IV
MEAN VALUE OF THE EXTRACTED PERMITTIVITY OF THE GETE AND GST OF ALL FABRICATED SAMPLES USING THE ANALYTICAL METHOD

Frequency	GeTe			GST
	Sample 1	Sample 2	Sample 3	Sample 4
20	19.7	22.2	26.3	32.7
30	20.6	22.0	25.9	32.4
40	19.5	22.3	26.2	32.6
50	18.0	20.7	26.0	30.0
60	20.7	22.7	25.8	34.3

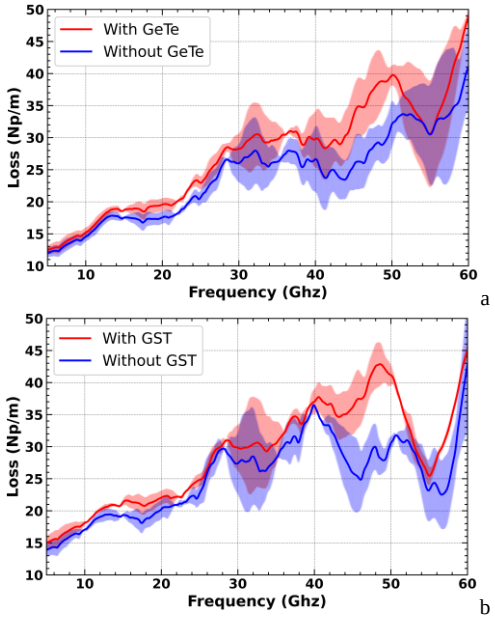

Fig. 11. (a) Comparison of the mean losses values extracted using the TRL method from a fabricated transmission line on alumina substrate with and without a GeTe layer of 800 nm (sample 2) and (b) for a fabricated transmission line on alumina substrate with and without a GST layer of 800 nm (sample 4).

The complete picture of frequency- dependent GeTe and GST permittivities is shown in Fig. 10(a) for GeTe and on Fig. 10(b) for GST, where it can be noticed that the permittivity values of both GeTe and GST, although having different values, are mostly constant over the investigated frequency band which supports the conclusions from the resonant method and strongly suggest that the permittivity of the GeTe and GST are little dispersive from 10 MHz up to 250 GHz [19]-[21].

The difference in the values of GeTe permittivity for the dissimilar samples 1-3 can be explained by errors introduced in the estimation of GeTe layers under a specific device, which may vary from the expected values across the surface of each sample (center to edges). Considering the small deviations from the expected values of the PCM thicknesses and the standard error of the mean permittivity values extracted from each line pairs, Fig. 10 shows also the dispersion of the permittivity values of the PCM layers.

Finally, Fig. 11(a) and Fig. 11(b) show a comparison of the losses of the CPW with and without a layer of PCM. From these figures, we can see that the addition of a very thin layer of PCM does have a noticeable impact on the losses of the CPW, however, the uncertainties associated with the measurement can make the extraction of the loss tangent of the PCMs difficult. Additionally, we notice that the uncertainties are increasing at

higher frequencies, which can be mostly attributed to the substrate roughness and local variations on the thickness of the PCM layers. Since the difference in the attenuation constant values from samples 1 and 3 is very small, they were not considered for the extraction of the loss tangent of the PCM. By comparing the shift on the real part of the propagation constant, from 3D electromagnetic retro simulation we can extract the loss tangent variation with frequency, as shown in Fig. 12(a) and Fig. 12(b). The extracted values of the loss tangent at 30 GHz for the GeTe and GST layers are of 3.4×10^{-2} and 3.2×10^{-1}, respectively.

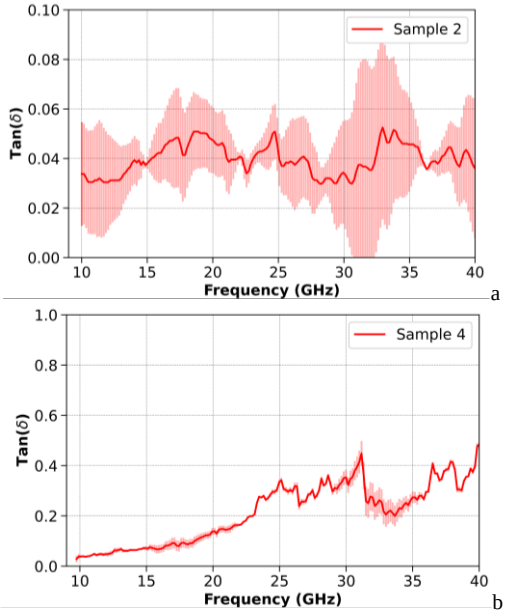

Fig. 12. (a) Mean and dispersion values of the extracted loss tangent of the GeTe from sample 2 and (b) of the GST from sample 4.

C. Results Synthesis And Discussions

From Table II and Table IV, it can be seen that the dielectric permittivity extracted from both methods agrees really well on average. Since the procedure for extracting the permittivity from the stubs resonators is very straightforward, these results allow us to cross-validate the results from the CPW method and post-processing required by the later.

From Fig. 10(a) and Fig. 10(b) one can notice that the permittivity of the PCM composition are mostly constant over the studied frequency bandwidth. The mean values recorded for the sample 3 (GeTe obtained on an optically polished SiO_2 substrate) produce a smother frequency-dependent permittivity curve, which can be explained by the fact that the surface of this substrate has a much lower roughness than the alumina ones (around 4 nm rms roughness against ~30 nm for alumina substrates). The extracted loss tangent values for the GeTe sample are mostly constant values, especially at low frequencies, nonetheless, the high roughness and variations of the layer thickness add a high degree of uncertainty to these values at high frequencies especially since the loss tangent value is low. For the GST composition, we can observe a monotonic increase of the loss tangent with increasing frequency. For both layers, the evaluated uncertainties can be greatly reduced by using longer lines with thicker PCM layers, on smoother substrates.

The results presented in Fig. 10(a) and the analysis of the permittivity dispersion values in Appendix III suggest that the devices fabricated on SiO_2 have the lowest dispersive permittivity values, followed by the devices fabricated on a thick (800 nm) GeTe layer (which may alleviate the initial roughness of the alumina substrate). The roughness of the substrate produces small local variations on the thickness of the PCM and therefore, induces a small change in the effective permittivity of the line. These changes are quantified in Appendix II and analyze in Appendix III. Assuming a nominal permittivity value of 22 for the GeTe composition and 32 for the GST composition, and using equations (36) and (38) (see annex II) we can estimate that for the extraction of the permittivity value within an error of 1%, the thickness of the PCM layer must be known within 10-nm precision for an alumina substrate. On the other hand, for a SiO_2 substrate, the thickness of the PCM must be known whiting 1-nm precision.

V. Conclusion

We proposed two different independent methods for evaluating the permittivity of very thin layers (less than 1 µm thick) of phase change materials when integrated in specific designs. The experimental results show that the addition of a PCM layer within the test devices has a sufficiently high impact on their behavior that can be quantified even if the thickness of the PCM composition is in the order of hundreds of nanometers. Although both methods provide similar results, the one based on the CPW allows the material characterization over a wide bandwidth while the resonant method only provides results at specific single frequencies. While the CPW method provides better results when the device is fabricated on a smooth and flat layer of the material under test, the resonator method requires the equalization of the ground planes using bonding wires (or metallic bridges) which may significantly impact the resonance frequency of the device. In addition, the CPW method allows the extraction of the losses of the line which can be used to deduce the loss tangent of the PCM film. However, the resonator method is much easier to implement since it only requires measuring the resonance frequency of the device, while the CPW method requires filtering of the data in addition to the implementation of a quasi-TRL methodology to extract the effective permittivity of the line. This adds substantial complexity to the use and implementation of the CPW method. These results represent one of the first reported values of permittivity for the GeTe and GST compositions in this broad frequency band (10 GHz to 60 GHz).

The comparison of the experimental results with analytical models and 3D electromagnetic simulations allowed to extract the dielectric properties of the material in the frequency range 10-60 GHz, but a precise knowledge of the dimensions of the CPW and the precise thickness of the PCM pattern is needed in order to accurately extract the permittivity of the PCM layers, in particular for the method based on stub resonators. Our results show that accurate characterization of PCM compositions using the presented methods requires devices integrating thick PCM layers obtained on smooth substrate and high permittivity. The results obtained from the CPW line method confirm previous studies on PCMs and will allow to implement the obtained dielectric properties in electromagnetic

simulations of more complex designs (antenna arrays, filters, switching networks, etc.).

APPENDIX I

The fundamental theory on the "Equivalent Network Representation" can be found at [28], [29], here we will present the steps to set up the equations to be solved to find the effective permittivity of a CPW line. Although this technique requires the circuit to be encapsulated in a metallic waveguide, the addition of this metallic walls should not perturb the behavior of the circuit provided that the circuit does not radiate and that the walls are sufficiently long from the circuit to study, therefore we consider that the circuit is encapsulated in a square waveguide of 1 mm side length. The electromagnetic structure to study is the one shown in Fig. 1(c) and Fig. 1(d), respectively, where w is the size of the gap, s is the width of the central line, h_s is the height of the substrate, and h_{pcm} is the thickness of the PCM layer deposed on the substrate. The substrate is characterised by its permittivity ε_r and the PCM is characterised by its permittivity ε_{PCM}.

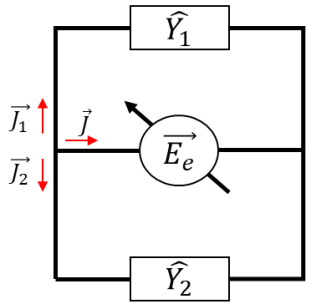

Fig. 13. Equivalent circuit representation of the coplanar waveguide shown in Fig. 1(c).

To transform the geometry of Fig. 1(c) and Fig. 1(d) to an equivalent network representation, we must first identify the boundary separating two regions of the space. For this case, this boundary is the plane where the metallization of the CPW is defined. This plane represents a mixed boundary (a plane where we have, at the same time, a conductive surface and a dielectric surface) that can be modelled as a variable source $\boldsymbol{E_e}$ (called "Virtual source") such that $\boldsymbol{E_e = 0}$ at the conductive surfaces (The CPW lines) and $\boldsymbol{E_e \neq 0}$ at the dielectric surface (the gap in the CPW). Is worth noticing that this virtual source does not deliver any power into the structure because the boundary conditions at the discontinuity plane impose that, in the metallic boundary the tangential electric field is zero and surface density current is non-zero, therefore the power delivered by the virtual source is zero. In the dielectric boundary, the tangential electric field is non-zero while the surface current density is zero and therefore the power delivered by the virtual source is, again, zero.

The boundary conditions imposed to the electromagnetic field at both sides of the boundary are represented by a dipole with an admittance operator $\hat{\boldsymbol{Y}}$ such that

$$\widehat{Y_i}\overrightarrow{E_e} = \vec{J_i} \tag{29}$$

where i is the considered region. This admittance operator is also characterised by the permittivity of the material in the considerate region. The general expression for the admittance operator is given by:

$$\widehat{Y_i} = \sum_n \left(|f_n^{TE}\rangle\, Y_{i,n}^{TE} \langle f_n^{TE}| + |f_n^{TM}\rangle\, Y_{i,n}^{TM} \langle f_n^{TM}| \right) \tag{30}$$

where $Y_{i,n}{}^{TE}$ and $Y_{i,n}{}^{TM}$ are given in [32] and the functions $f_n{}^{TE}$ and $f_n{}^{TM}$ are the modal basis functions given in [28] for the TE and TM modes in the waveguide. The precise form of the admittance operators is given in our principal discussion as their particular form depends on if the structure is a single layer or multilayer substrate.

Finally, the virtual source and the dipoles can be joined together to form the circuit represented in Fig. 13.

The application of Kirchhoff's and Ohm laws to the circuit in Fig. 13 gives the following equation:

$$\left(\widehat{Y_1} + \widehat{Y_2}\right)\overrightarrow{E_e} = \vec{J}. \tag{31}$$

But because $\boldsymbol{E_e}$ is zero when $\boldsymbol{J}$ is non-zero (and vice versa), (31) reduces to:

$$\left(\widehat{Y_1} + \widehat{Y_2}\right)\overrightarrow{E_e} = 0 \tag{32}$$

Equation (32) represents an integral equation that can be solved applying Galerkin's method by decomposing the virtual source $\boldsymbol{E_e}$ into a set of trial functions $\boldsymbol{g_e}$ defined such that:

$$\overrightarrow{E_e} = v_e \overrightarrow{g_e} \tag{33}$$

where v_e is designated unknown coefficients and $\boldsymbol{g_e}$ is defined as:

$$\overrightarrow{g_e} = \begin{cases} g_{ex} = \begin{cases} -1 \; for \; x \in \left[\frac{a-s}{2} - w, \frac{a-s}{2}\right] \\ +1 \; for \; x \in \left[\frac{a+s}{2}, \frac{a+s}{2} + w\right] \\ 0 \qquad\qquad elsewhere \end{cases} \\ g_{ez} = 0 \qquad for \; x \in [0, a] \end{cases} \tag{34}$$

Note that g_{ex} represents a rough approximation of an odd mode propagating in the CPW line. The fact the g_{ez} is zero means that we are consideration a pure TEM mode in the line.

Then (32) has a solution, other than the trivial one ($v_e = 0$), if and only if

$$\left\langle \overrightarrow{g_e} \middle| \left(\widehat{Y_1} + \widehat{Y_2}\right) \overrightarrow{g_e} \right\rangle = 0 \tag{35}$$

where $\langle . | . \rangle$ represents the Hermitian scalar product.

APPENDIX II

The accuracy of the proposed procedure to extract the permittivity of the PCM lies in the fact that one can accurately deduce the effective permittivity of the device using either (13) or (1). Therefore, it is of interest to evaluate how small changes in the parameters of the deposed layer of PCM may affect the effective permittivity of the line. For this purpose, we can calculate the partial derivative of the effective permittivity of the coplanar line device with respect to different parameters of the PCM using either (13) or 3D electromagnetic simulation. The partial derivatives were calculated numerically using the nominal parameters of the CPW line.

The first quantity of interest is how sensitive is the effective permittivity of the CPW to the permittivity of the obtained PCM. The changes of ε_{PCM} due to small changes in ε_{eff} can be calculated using

$$\Delta\varepsilon_{PCM} = \Delta\varepsilon_{eff} \left(\frac{\partial \varepsilon_{eff}}{\partial \varepsilon_{PCM}}\right)^{-1}. \tag{36}$$

As an example, a CPW with a PCM thickness of 500 nm, has a numerical value for the partial derivative of 0.021 using the analytical method and 0.019 using the 3D EM simulation. Then, using (36), we can deduce that an error of 0.1 in the ε_{eff} produces an error of 5 in the value of ε_{PCM}.

The uncertainty on the effective permittivity due to small deviations on the parameters of the can be evaluated using:

$$\Delta\varepsilon_{eff} = \sqrt{\left(\Delta h_{PCM}\frac{\partial\varepsilon_{eff}}{\partial h_{PCM}}\right)^2 + \left(\Delta s\frac{\partial\varepsilon_{eff}}{\partial s}\right)^2 + \left(\Delta w\frac{\partial\varepsilon_{eff}}{\partial w}\right)^2 + \left(\Delta h_s\frac{\partial\varepsilon_{eff}}{\partial h_s}\right)^2} \quad (37)$$

where Δh_{pcm}, Δs, Δw, Δh_s are small changes in the thickness of the PCM, the width of the central conductor of the CPW, the gap of the CPW and the height of the substrate, respectively. Since optical lithography presents an accuracy of around 1 µm, and the devices were fabricated on substrates cut from the same wafer and lithographically processed at the same time, the terms Δs and Δw can be neglected. Moreover, since the height of the substrate is much bigger than the dimensions of the CPW, small variations of its value can be neglected also. Therefore, (37) can be written as:

$$\Delta\varepsilon_{eff} = \Delta h_{PCM}\frac{\partial\varepsilon_{eff}}{\partial h_{PCM}}. \quad (38)$$

This means that the uncertainties in the value of the effective permittivity of the line can be attributed mostly to uncertainties in the thickness of the PCM layer. A similar analysis can be done for the attenuation constant of the CPW by replacing ε_{eff} *with* α_t.

For the stub resonators, there is an additional parameter: the length of the resonator which can be solved analytically taking the partial derivative of (1):

$$\frac{d\varepsilon_{eff}}{dL} = -2\frac{\varepsilon_{eff}^n}{L} \quad (39)$$

where ε_{eff}^n is the effective permittivity calculated from (1) using the nominal values of the resonators. From (39), we can see that a larger resonator is less sensitivity to smalls variations of the length of the resonator.

APPENDIX III

In Appendix II, it is stated that small deviations on the geometry of the CPW will affect the value of the effective permittivity of the line and therefore introduce errors in the extracted permittivity of the PCM. These errors are calculated using (36), (37) and (38) which requires the evaluation of partial derivatives. Since we do not dispose of an explicit equation for evaluating the value of the partial derivatives, these values were calculated numerically from (15) by adding small perturbations to the geometric parameters of the CPW and looking at their influence in the effective permittivity of the line. The numerical values of the partial derivatives are shown, for each sample, in Table V from which it can be noticed that sample 4 is the most sensitive to errors in the thickness of the deposed PCM, which can be attributed to the low permittivity of the substrate. From samples 1 and 2 we observe that their sensitivity to errors in thickness of the PCM layer is independent of the thickness of the layer (sample 1 has a nominal PCM thickness of 500 nm and sample 2 has a nominal PCM thickness of 800 nm). But this sensitivity is inversely proportional to the permittivity of the substrate, which can be seen from sample 4 (GeTe over a SiO_2 substrate) who has a smaller permittivity value than the alumina substrate. From samples 2 (800 nm thick GeTe layer) and 4 (800 nm thick GST layer), we can observe that the bigger the permittivity of the PCM, the more sensible is the effective permittivity to deviations on the thickness of the PCM.

TABLE V.

SENSITIVITY OF THE EFFECTIVE PERMITTIVITY OF THE PCM FOR ALL SAMPLES USING THE ANALYTICAL METHOD

Sample	$\left(\frac{\partial\varepsilon_{eff}}{\partial\varepsilon_{PCM}}\right)^{-1}$	$\frac{\partial\varepsilon_{eff}}{\partial h_{PCM}}$ (µm)$^{-1}$
1	66.7	0.336
2	41.7	0.348
3	76.9	2.68
4	50.0	0.654

The sensitivity of the extracted permittivity of the PCM to errors in the effective permittivity is quantified by (36) which requires knowledge of the derivative of effective permittivity to the permittivity of the PCM. Comparing sample 1 and sample 3, we conclude that the lower the permittivity of the substrate, the more sensible is the extracted value of the PCM to errors in the value of the effective permittivity. From samples 1 and 2 we observe that, the bigger the thickness of the PCM layer, the smaller the sensitivity of the extracted PCM permittivity. While from samples 2 and 4, we note that the bigger the permittivity of the PCM, the more sensitive is the extracted permittivity of the PCM to errors in the value of the effective permittivity.

REFERENCES

[1] S. Chen and J. Zhao, "The requirements, challenges, and technologies for 5G of terrestrial mobile telecommunication," in *IEEE Commun. Mag.*, vol. 52, no. 5, pp. 36-43, May, 2014, doi: 10.1109/MCOM.2014.6815891.

[2] E. Dahlman *et al*., "5G wireless access: requirements and realization," in *IEEE Commun Mag.*, vol. 52, no. 12, pp. 42-47, Dec., 2014, doi: 10.1109/MCOM.2014.6979985.

[3] M. Marcus and B. Pattan, "Millimeter wave propagation: spectrum management implications," in *IEEE Microw. Mag.*, vol. 6, no. 2, pp. 54-62, June, 2005, doi: 10.1109/MMW.2005.1491267.

[4] W. A. Awan, A. Zaidi, N. Hussain, S. Khalid, Halima and A. Baghdad, "Frequency Reconfigurable patch antenna for millimeter wave applications," in *2019 2nd Int. Conf. on Comput., Math. and Eng. Technol.*, Sukkur, Pakistan, 2019, pp. 1-5, doi: 10.1109/ICOMET.2019.8673417.

[5] J. Balcells, Y. Damgaci, B. A. Cetiner, J. Romeu and L. Jofre, "Polarization reconfigurable MEMS-CPW antenna for mm-wave applications," in *Proc. 4th Eur. Conf. Antennas. Propag.*, Barcelona, Spain, 2010, pp. 1-5.

[6] P. -Y. Qin, A. R. Weily, Y. J. Guo and C. -H. Liang, "Millimeter wave frequency reconfigurable quasi-Yagi antenna," in *2010 Asia Pacific Microw. Conf.*, Yokohama, Japan, 2010, pp. 642-645.

[7] H. Shimasaki and T. Itoh, "Experimental study on the radiation beam scan of a waveguide slot array antenna filled with a ferrite," in *2006 Asia-Pacific Microw. Conf.*, 2006, pp. 2118-2121, doi: 10.1109/APMC.2006.4429831

[8] D. E. Anagnostou, T. S. Teeslink, D. Torres and N. Sepúlveda, "Vanadium dioxide reconfigurable slot antenna," in *2016 IEEE Int. Symp. Antennas Prop.*, Fajardo, PR, USA, 2016, pp. 1055-1056, doi: 10.1109/APS.2016.7696235.

[9] M. Agaty, A. Crunteanu, C. Dalmay and P. Blondy, "Ku Band High-Q Tunable Cavity Filters using MEMS and Vanadium Dioxide (VO2) Tuners," in 2018 *IEEE MTT-S Int. Microw. Workshop Ser. Adv. Mater. Processes RF. THz. Appl.*, Ann Arbor, MI, USA, 2018, pp. 1-3, doi: 10.1109/IMWS-AMP.2018.8457138.

[10] N. El-Hinnawy, G. Slovin, C. Masse, P. Hurwitz, J. Rose and D. Howard, "Switch Stacking for OFF-State Power Handling Improvements in PCM RF Switches," in *2021 IEEE MTT-S Int. Microw. Symp.*, 2021, pp. 424-427, doi: 10.1109/IMS19712.2021.9574954.

[11] A. Crunteanu, L. Huitema, J. Orlianges, C. Guines and D. Passerieux, "Optical switching of GeTe phase change materials for high-frequency applications," in *2017 IEEE MTT-S Int. Microw. Workshop Ser. Adv. Mater. Processes RF. THz. Appl.*, Pavia, Italy, 2017, pp. 1-3, doi: 10.1109/IMWS-AMP.2017.8247379.

[12] A. Mennai, A., Bessaudou, F. Cosset, C. Guines, P. Blondy, A. Crunteanu, "Bistable RF Switches Using Ge2Sb2Te5 Phase Change Material", in *18th Eur. Microw. Week*, Paris, France, pp. 1-4, 2015.

[13] N. El-Hinnawy *et al*., "Substrate agnostic monolithic integration of the inline phase-change switch technology," in *IEEE MTT-S Int. Microw. Symp.*, San Francisco, CA, USA, 2016, pp. 1-4, doi: 10.1109/MWSYM.2016.7540103.

[14] L. Chau et al., "Optically controlled GeTe phase change switch and its applications in reconfigurable antenna arrays", in *Proc. SPIE. Open Archit./Open Bus. Model Net Centric Syst. Defense Transformation*, 2015.

[15] A. Crunteanu, A. Mennai, C. Guines, D. Passerieux and P. Blondy, "Out-of-plane and inline RF switches based on Ge2Sb2Te5 phase-change material," in *2014 IEEE MTT-S Int. Microw. Symp.*, Tampa, FL, USA, 2014, pp. 1-4, doi: 10.1109/MWSYM.2014.6848417.

[16] Y. C. Chen *et al*., "Ultra-Thin Phase-Change Bridge Memory Device Using GeSb," in 2006 *IEEE Int. Electron Devices Meeting*, San Francisco, CA, USA, 2006, pp. 1-4, doi: 10.1109/IEDM.2006.346910.

[17] A. Ghalem, C. Guines, D. Passerieux, J. -C. Orlianges, L. Huitema and A. Crunteanu, "Reversible, Fast Optical Switching of Phase Change Materials for Active Control of High-Frequency Functions," *2018 IEEE/MTT-S Int. Microw. Symp.*, Philadelphia, PA, USA, 2018, pp. 839-842, doi: 10.1109/MWSYM.2018.8439247.

[18] J. L. Valdes, L. Huitema, E. Arnaud, D. Passerieux and A. Crunteanu, "A Polarization Reconfigurable Patch Antenna in the Millimeter-Waves Domain Using Optical Control of Phase Change Materials," in *IEEE Open J. Antennas Propag.*, vol. 1, pp. 224-232, 2020, doi: 10.1109/OJAP.2020.2996767.

[19] C. Chen, P. Jost, H. Volker, M. Kaminski, M. Wirtssohn, U. Engelmann, K. Krüger, F. Schlich, C. Schlockermann, R. P. S. M. Lobo, and M. Wuttig, "Dielectric properties of amorphous phase-change materials", in *Phys. Rev. B*, vol. 95, 2017, doi: 10.1103/PhysRevB.95.094111.

[20] E. Prokhorov, J. J. Gervacio-Arciniega, G. Luna-Bárcenas, Y. Kovalenko, F. J. Espinoza-Beltrán, and G. Trápaga, "Dielectric properties of Ge2Sb2Te5 phase-change films," in *J. Appl. Phys.*, vol. 113, 2013, doi: 10.1063/1.4795592.

[21] F. Kadlec, C. Kadlec, P. Kužel, "Contrast in terahertz conductivity of phase-change materials", in *Solid State Commun.*, vol. 152, doi.org/10.1016/j.ssc.2012.02.018

[22] V. Bovtun *et al*., "Microwave characterization of dielectric substrates for thin films deposition," in *2013 IEEE XXXIII Int. Scientific Conf. Electron. Nanotechnol.*, Kiev, Ukraine, 2013, pp. 17-20, doi: 10.1109/ELNANO.2013.6552081.

[23] C. D. Easton, M. V. Jacob, and J. Krupka, "Non-destructive complex permittivity measurement of low permittivity thin film materials," in Meas. Sci. Technol., vol. 18, no. 9, pp. 2869–2877, Jul. 2007, doi: 10.1088/0957-0233/18/9/016.

[24] U. C. Hasar, "Determination of Complex Permittivity of Low-Loss Samples From Position-Invariant Transmission and Shorted-Reflection Measurements," in *IEEE Trans. Microw. Theory Tech.*, vol. 66, no. 2, pp. 1090-1098, Feb. 2018, doi: 10.1109/TMTT.2017.2772864.

[25] U. C. Hasar, Y. Kaya, J. J. Barroso and M. Ertugrul, "Determination of Reference-Plane Invariant, Thickness-Independent, and Broadband Constitutive Parameters of Thin Materials," in *IEEE Trans. Microw. Theory Tech.*, vol. 63, no. 7, pp. 2313-2321, July 2015, doi: 10.1109/TMTT.2015.2431685.

[26] V. Laur *et al*., "Wide-Band Characterization of Ferroelectric Thin-Films: Applications to KTN-based Microwave Agile Devices," *2006 Eur. Microw. Conf.*, Manchester, UK, 2006, pp. 929-932, doi: 10.1109/EUMC.2006.281073.

[27] R. B. Marks, "A multiline method of network analyzer calibration," in *IEEE Trans. Microw. Theory Tech.*, vol. 39, no. 7, pp. 1205-1215, July 1991, doi: 10.1109/22.85388.

[28] H. Baudrand, "Representation by Equivalent circuit of the Integral methods in Microwave passive elements," in *1990 20th Eur. Microw. Conf.*, 1990, pp. 1359-1364, doi: 10.1109/EUMA.1990.336256.

[29] H. Baudrand, H. Aubert, D. Bajon, and F. Bouzidi, "Equivalent network representation of boundary conditions involving generalized trial quantities," in *Ann. Télécommun.*, vol. 52, no. 5–6, pp. 285–292, May 1997, doi: 10.1007/BF02996071.

[30] F. Bouzidi, H. Aubert, D. Bajon and H. Baudrand, "Equivalent network representation of boundary conditions involving generalized trial quantities-application to lossy transmission lines with finite metallization thickness," in *IEEE Trans. Microw. Theory Tech.*, vol. 45, no. 6, pp. 869-876, June 1997, doi: 10.1109/22.588594.

[31] F. Bouzidi, H. Aubert, D. Bajon, H. Baudrand, and V. F. Hanna, "Equivalent circuit representation of lossy coplanar waveguides," in Ann. Télécommun., vol. 47, no. 11, pp. 551–554, Nov. 1992, doi: 10.1007/BF02998323.

[32] T. Itoh, "Spectral Domain Immitance Approach for Dispersion Characteristics of Generalized Printed Transmission Lines," in *IEEE Trans. Microw. Theory Tech.*, vol. 28, no. 7, pp. 733-736, Jul. 1980, doi: 10.1109/TMTT.1980.1130158.

[33] Y. Morimoto, T. Motegi, W. Kasai and K. Niwano, "Transmission Line Loss Properties of Dielectric Loss Tangent and Conductive Surface Roughness in 5G Millimeter Wave Band," in *2020 IEEE Asia-Pacific Microw. Conf.*, Hong Kong, Hong Kong, 2020, pp. 776-778, doi: 10.1109/APMC47863.2020.9331571.

[34] X. Guo, D. R. Jackson and J. Chen, "An analysis of copper surface roughness effects on signal propagation in PCB traces," in *2013 Texas Symp. Wireless Microw. Circuits Syst.*, Waco, TX, USA, 2013, pp. 1-4, doi: 10.1109/WMCaS.2013.6563552.

[35] Chung-Yi Lee, Yaozhong Liu and Tatsuo Itoh, "The effects of the coupled slotline mode and air-bridges on CPW and NLC waveguide discontinuities," in *IEEE Trans. Microw. Theory Tech.*, vol. 43, no. 12, pp. 2759-2765, Dec. 1995, doi: 10.1109/22.475632.

[36] N. I. Dib, M. Gupta, G. E. Ponchak and L. P. B. Katehi, "Characterization of asymmetric coplanar waveguide discontinuities," in *IEEE Trans. Microw. Theory Tech.*, vol. 41, no. 9, pp. 1549-1558, Sept. 1993, doi: 10.1109/22.245676.

[37] Abraham. Savitzky and M. J. E. Golay, "Smoothing and Differentiation of Data by Simplified Least Squares Procedures.," in Anal. Chem., vol. 36, no. 8, pp. 1627–1639, Jul. 1964, doi: 10.1021/ac60214a047.